Long-Range LiDAR and Free-Space Data Communication with High-Performance Optical Phased Arrays

Christopher V. Poulton, Matthew J. Byrd, Peter Russo, Erman Timurdogan, Murshed Khandaker, Diedrik Vermeulen, and Michael R. Watts

(Invited Paper)

***Abstract*—We present high-performance integrated optical phased arrays along with first-of-their-kind LiDAR and free-space data communication demonstrators. First, record-performance optical phased array components are shown with low-power phase shifters and high-directionality waveguide grating antennas. Then, one-dimensional 512-element optical phased arrays are demonstrated with record low power operation (<1 mW total), large steering ranges, and high-speed two-dimensional beam steering (<30 µs phase shifter time constant). Next, by utilizing optical phased arrays, we show coherent 2D solid-state LiDAR on diffusive targets with simultaneous velocity extraction at a range of nearly 200 m. In addition, the first demonstration of 3D coherent LiDAR with optical phased arrays is presented with raster-scanning arrays. Finally, lens-free chip-to-chip free-space optical communication links up to 50 m are shown, including a demonstration of a steerable transmitter to multiple optical phased array receivers at a 1 Gbps data rate. This work shows the most advanced silicon photonics solid-state beam steering to date with relevant demonstrators in practical applications.**

***Index Terms*—Silicon photonics, optical phased arrays, solid-state beam steering, LiDAR, free-space data communication.**

I. Introduction

INTEGRATED optical beam steering with photonic integrated circuits (PIC) has become a crucial technology with the capability to produce fast-scanning low-divergence beams. A variety of on-chip beam steering techniques have been proposed such as planar lenses [1], reflective optical microelectromechanical systems (MEMS) [2], and integrated optical phased arrays (OPA) [3]. Integrated OPAs are a particularly attractive solution due to their ability to create a large out-of-plane-emitting conformal aperture and completely solid-state operation. Much like their well-established radio frequency counterparts used in RADAR and communications, OPAs achieve beam forming by tuning the phases of arrayed antennas in order to alter the phase front of the emitted beam. OPA aperture sizes of many millimeters are possible [4], producing diffraction-limited beams with sub-milliradian divergence angles and large-area receivers. Combined with standard integrated photonic components, such as modulators and detectors, PICs with OPAs have the potential to realize chip-scale systems for a wide variety of applications requiring beam steering.

Originally introduced in silicon photonics by K.V. Acoleyen *et al.* in 2009 [5], [6], [7], OPAs saw tremendous progress in scale, performance, and system integration as demonstrated by the work of J. Sun *et al.* [8], [9], [10], [11] a few years later. In addition to conventional silicon photonics, OPAs have been implemented in a variety of integrated photonics platforms, each with its own benefits, such as InP [12], III/V hybrid platforms [13], commercial CMOS processes with monolithic electronics and photonics [14], [15], and custom processes with integrated erbium-doped lasers [16]. The rise of mature foundry-enabled PICs [17] has facilitated increasingly complex OPA demonstrations with direct applications ranging from light detection and ranging (LiDAR) [18], free-space data communication [19], [20], [21], [22], [23], cameras [24], [25], [26], [27], and image projection [28], [29].

LiDAR, due to the vastly improved diffraction limit offered by optical waves, provides much higher angular resolution images than RADAR and is thus widely used in autonomous systems. Due to the emerging need for solid-state LiDARs to increase durability while reducing size and cost, there is significant interest in implementing OPA-based LiDAR. This is an opportunity for integrated photonics to intersect a massive market which has not previously employed the technology. Furthermore, OPAs are well suited for free-space optical (FSO) data communication applications, in order to increase transceiver deployment in size, weight, power, and cost (SWaP-C) constrained environments. This communication-centered application is a natural fit for silicon photonic technology which is currently revolutionizing the datacom and telecom industries with tightly-integrated high-speed modules.

In this work, we present high-performance integrated optical phased arrays along with LiDAR and free-space data communication demonstrations fabricated on 300 mm SOI wafers in a silicon photonics process. First, record-performance OPA components are shown including tightly-pitched phase shifters with microwatt-level power consumption and low 2.4 dB av-

Manuscript received XXX, 2018; revised YYY, 2019; accepted ZZZ, 2019. This work was supported by the Defense Advanced Research Projects Agency (DARPA) of the United States under the Modular Optical Aperture Building Blocks (MOABB) program under grant number HR0011-16-C-0108. The views, opinions and/or findings expressed are those of the author and should not be interpreted as representing the official views or policies of the Department of Defense or the U.S. Government. Released under Distribution Statement "A" (Approved for Public Release, Distribution Unlimited).

The authors are with Analog Photonics, Boston, MA 02110 USA (email: cpoulton@analogphotonics.com; mbyrd@analogphotonics.com; peter@analogphotonics.com; erman@analogphotonics.com; mkhandaker@analogphotonics.com; diedrikv@analogphotonics.com; mwatts@analogphotonics.com.

erage loss, and multi-millimeter-scale waveguide grating antennas with >90% directionality over a ∼200 nm band. Afterwards, by combining these components, one-dimensional 512-element OPAs are demonstrated with inline pitches as low as 1.65 µm. The matched phase shifter and antenna pitch enables an inline architecture with an inherently scalable design and high aperture fill factor. These OPAs are capable of low power operation (<1 mW total), large steering range (56°×15°), and high-speed beam steering (<30 µs phase shifter time constant). A steerable beam with a FWHM diffraction angle of 0.04° is shown with 12 dB side lobe suppression and <25 dB noise floor for high power-in-main-beam efficiency. Next, using OPAs, a coherent LiDAR system is demonstrated on diffusive targets with simultaneous distance and velocity measurements. This system is taken outside and 2D LiDAR is achieved at a 185 m range. Additionally, 3D LiDAR is realized with active raster-scanning OPAs, demonstrating 3D coherent LiDAR with OPAs for the first time. Finally, we present lens-free OPA-to-OPA free-space optical links, paving the way for OPA-based FSO communication. Specifically, we show a static 50 m point-to-point link at a data rate of 10 Gbps using two passive OPAs, and the first point-to-multipoint communication link at 1 m with a 1 Gbps data rate using an active OPA transmitter steering between multiple OPA receivers.

II. Optical Phased Array Architecture

Figure 1(a) is a rendering of a one-dimensional OPA architecture [30]. The major components include an optical distribution network to an array of elements, optical phase shifters, and out-of-plane emitting antennas. The optical distribution network converts a single-mode input waveguide to a set of N elements. To design an optical distribution network without fan-in/fan-out sections, the output distribution pitch should be matched to the element pitch. The estimated loss of the splitter network is 0.6 dB. After distribution, each element has an individually controlled phase shifter. This is unlike previous work which utilizes architectures such as cascaded phase shifters [18], [31] or row-column-based phase shifters [15]. There, groups of elements are tied to a single electrical line and portions of the emission wavefront cannot be independently controlled. Individual element phase control enables increased flexibility of the emitted wavefront at the cost of increased control complexity. Finally, each element has a multi-millimeter-scale waveguide grating antenna for out-of-plane emission [32], [33], [34] (instead of in-plane or end-fire emission [35]). A long antenna length increases the directivity of the emitter and enables a narrow element factor in the orthogonal dimension of the one-dimensional array factor. Moreover, a grating-based emitter has an inherent wavelength/angle dependence that enables two-dimensional beam steering with wavelength tuning. Though a tunable light source increases system complexity, wavelength steering enables 1D OPAs to have similar functionalities as 2D OPAs, while having orders of magnitude less elements for a given aperture size, decreasing I/O count and power consumption.

With element counts reaching into the thousands, low-power phase shifters are essential. Here, broadband electro-optic phase shifters are used over thermal phase shifters for their low power consumption, minimal cross-talk to adjacent elements, and high electrical bandwidths. Figure 1(b) shows the measured loss and power consumption of an individual OPA phase shifter structure. A phase shift of 2π is achieved with a low average loss of 2.4 dB when applying modulo 2π across the elements (this loss is similar throughout the C+L band). The maximum static power consumption of the phase shifter is only 2 µW, which is orders of magnitude less than thermo-optic phase shifters, which can require generally require >10 mW of power, and even when optimized need

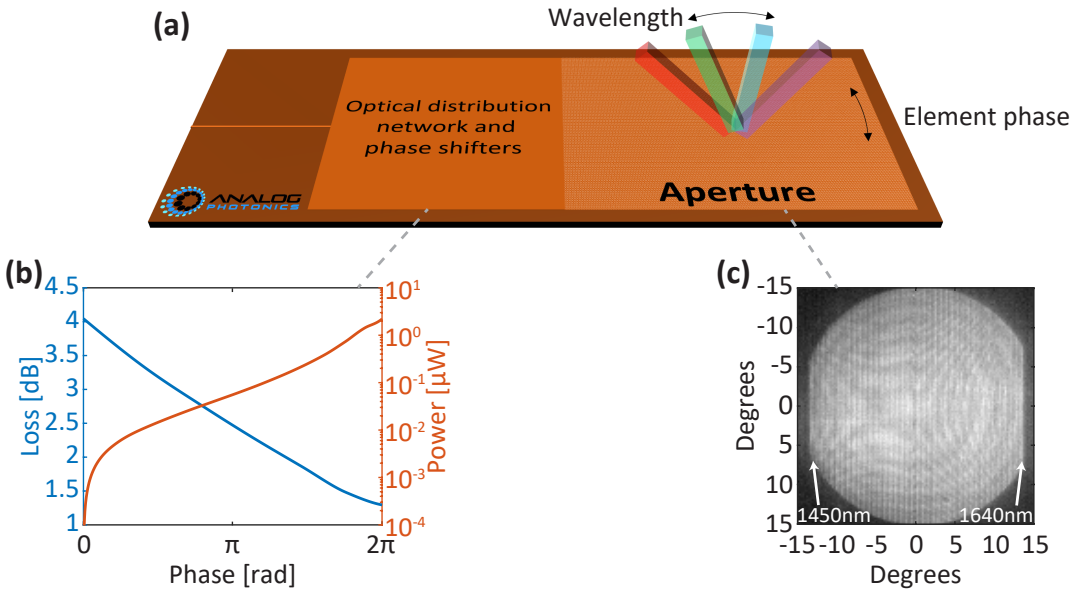

Fig. 1: (a) Architecture of a one-dimensional optical phased array consisting of an optical distribution network, optical phase shifters, and out-of-plane emitters. (b) Measured optical phase shifter loss and power consumption. (c) Sum of element factors while tuning wavelength showing minimal interaction with the silicon substrate.

>1 W of power for a 512-element OPA [36]. Furthermore, the phase shifters are pitch-matched with the emitting elements for an inline OPA architecture. Inline architectures are inherently scalable to thousands of elements and minimize the footprint of components or pitch-converting-structures that are not part of an emitting aperture. A low aperture fill factor increases die cost, and can fundamentally limit aperture size. Finally, a long unidirectional waveguide grating antenna design with optical perturbations is employed for maximum efficiency and minimum distortion from downwards emission. Any downwards emission from the antennas reflects off the silicon substrate which can be observed through fringes in the element factor [34]. Figure 1(c) plots a sum of element factors while sweeping wavelength. The depth of the far field pattern fringes, ~1 dB, indicate the antennas have greater than 90% upwards directionality, even with wavelength steering from 1450 nm to 1640 nm. Though this is an approximate measurement, it matches the simulated >93% upwards directionality over the same wavelength band.

III. Integrated Beam Steering

The high-performance components described in Section II can be combined into an OPA PIC such as the one shown in Fig. 2. This OPA has a large 512-element count and an aperture area of ~10 mm^2. The chip is die-attached to a PCB and wirebonded to PCB pad sites, which are fanned out to control electronics consisting of DACs and an FPGA with custom firmware. Optical packaging includes epoxying a polarization maintaining fiber to the input on-chip mode-converter. After packaging, the phase distribution of the elements is calibrated and a look-up-table (LUT) is generated for beam steering. Figure 3(a) plots a cross-section of the far field in the phased array dimension measured from the device after calibration. A full-width at half-maximum diffraction angle of less than 0.04° (700 µrad) is measured, closely matching theory as does the magnitude of the side lobes. Some of the deviation from theory

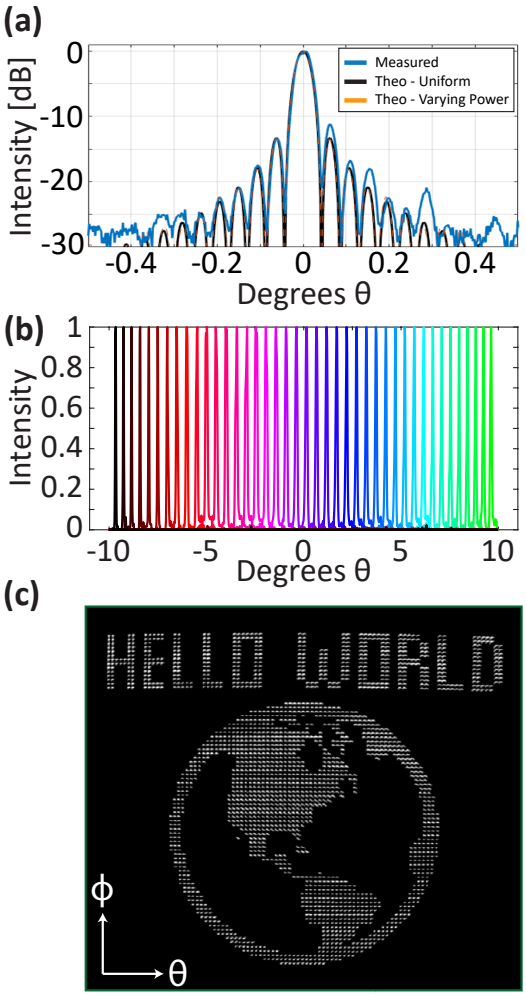

Fig. 3: (a) Cross-section of the far field in the phase shifter dimension showing close agreement with theory. (b) Beam steering with phase shifters in one dimension, limited by optical setup NA. (c) Sum of far field spots showing 2D beam steering with phase shifters (θ) and input wavelength (ϕ).

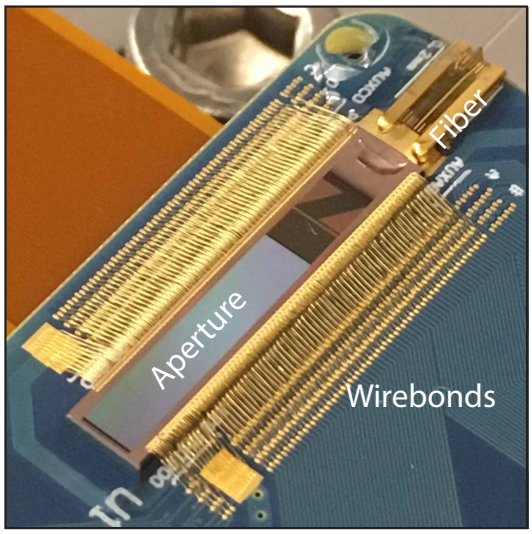

Fig. 2: Electrically and optically packaged 512-element optical phased array with an inline architecture.

can be explained because the varying optical attenuation of the phase shifters causes the theoretical higher-order side-lobes to vary slightly compared to the uniform power distribution theoretical curve, but the main beam and first-order side-lobes remain similar. More importantly, the theoretical main beam peak is ~2.4 dB (the average phase shifter loss) lower than the lossless and ideal optical phased array. A side lobe suppression of 12 dB is measured with a noise floor of around –25 dB (measurement limited by dynamic range of IR camera). This indicates a high-fidelity calibration algorithm and phase shifter yield (expected to be larger than 95%). The major contribution to yield is predicted to be packaging related.

Figure 3(b) shows far field intensity cuts when beam steering with the optical phase shifters in a 20° field of view, limited by the NA of the optical setup used for far field imaging. The beam profile has a similar emission pattern while steering, showing the effectiveness of the calibration algorithm and the uniformity of the optical phase shifters. The large element count and aperture of the OPA facilitates

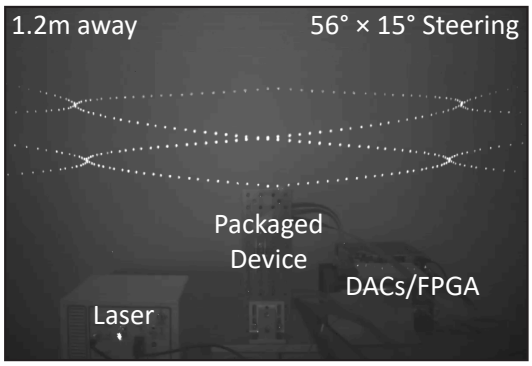

Fig. 4: IR camera image of the sum of spots in a "figure-8" pattern formed by a packaged optical phased array incident to a wall 1.2 m away. An inline pitch of 1.65 µm and wavelength steering produced a steering range of 56°×15°.

high-resolution scan patterns. Figure 3(c) is a sum of various normalized far field spots when performing 2D beam scanning with the phase shifters (θ) and input wavelength (ϕ). Note that no adjustment to the element phase values is needed while performing wavelength steering due to the OPA architecture (though beam squint causes slight inwards/outwards steering while changing wavelength). This enables a one-dimensional LUT with minimal memory requirements, and potentially increases two-dimensional raster scanning rates due to truly independent wavelength and phase steering. Moreover, the phased array operation of the device enables completely random-access scan patterns which is useful for increasing the point density in a certain location within a LiDAR field of regard.

Figure 4 shows an IR camera image of the sum of spots in a repeated "figure-8" scan pattern formed by an OPA incident to a wall 1.2 m away. A wall is used instead of a far field imaging setup to conveniently show the steering range of the device in an applicable environment. The figure shows the laser, DACs, and FPGA driving the packaged OPA. Discretized points are seen in the pattern due to the FPGA having an on-board memory limit of ∼200 points in the LUT, which can be greatly increased by using external SRAM. Point-to-point steering speeds of ∼30 µs were achieved in the phase dimension, limited by the interface between the FPGA and DACs. A steering range of 56°×15° is shown, facilitated by the inline 1.65 µm pitch of the elements. Beam aliasing and the formation of grating lobes fundamentally limits the steering range due to the uniformly-pitched elements placed at $>\lambda/2$ and thus an aliased pattern is seen at ±28°. At broadside, the grating lobe loss was ∼1 dB. Using an aperiodic pitch can increase the steering range at the cost of an increased background noise and lower main beam efficiency [3], [37].

IV. LiDAR with Integrated Optical Phased Arrays

Integrated OPAs offer an interesting solution for LiDAR applications by enabling solid-state beam steering PICs with flat conformal apertures and near-arbitrary control. By utilizing mature high-performance silicon photonic platforms, which contain a wide variety of components such as filters, modulators, and detectors, OPA-based LiDAR systems have the potential to realize tightly-integrated, inexpensive, and mass-producible solid-state LiDARs on 300 mm silicon wafers. A unique advantage of integrated photonics is the simplicity of implementing coherent detectors. This enables coherent LiDAR detection modalities as opposed to time-of-flight (TOF) techniques. Coherent LiDAR offers a variety of fundamental advantages to TOF LiDAR such as insensitivity to ambient light, shot-noise limited performance, higher dynamic range, and moderate peak powers. Moreover, it can simultaneously measure the distance and velocity of a target by detecting an imparted Doppler frequency, such as in frequency-modulated continuous-wave (FMCW) LiDAR [38] which utilizes a bi-directional chirped laser. Note that, OPAs transmit and receive in a single polarization so rotations caused by reflections can reduce a LiDAR signal. 2D LiDAR systems can be realized with 1D-scanning beam steering to range objects over a single angular dimension. However, to measure a solid-angle, a 3D LiDAR system must be created with a 2D-scanning beam steerer. In addition, multiple 3D LiDAR systems can be concatenated to cover the required field-of-view for a given application.

First, a prototype LiDAR system was created with two large-scale passive OPAs (without phase shifters), along with fiber-based components such as couplers, detectors, and an external C+L band commercial-off-the-shelf tunable laser. The type of the laser is a table-top swept-wavelength external-cavity diode

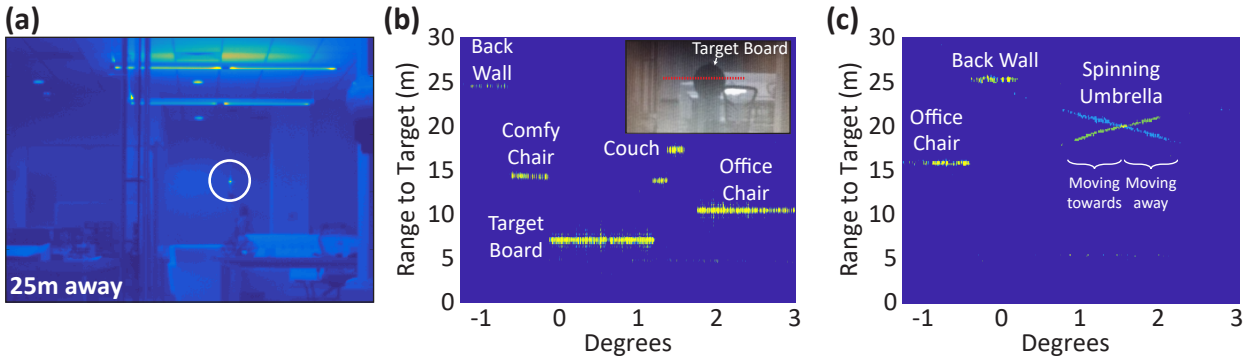

Fig. 5: (a) Beam of large-scale passive OPA on a wall 25 m away. (b) LiDAR ranging results on diffusive targets, inset shows ranged scene and scan line. (c) LiDAR detections on a spinning target showing velocity sensing of magnitude and direction.

Fig. 6: (a) Map of outdoor scene scanned by 2D LiDAR system. (b) Real-time visualization of output LiDAR data showing detections at a 185 m range (color is representative of range).

laser. Figure 5(a) is an IR camera image of the beam emitted from the transmitter OPA on a wall 25 m away. Even though the OPAs are passive, solid-state beam steering and 2D LiDAR can be performed by tuning the input wavelength. LiDAR detections up to 25 m were achieved, limited by the room size, as shown in Fig. 5(b). Ranged targets include common diffuse objects such as walls, chairs, and couches.

In addition, Doppler frequency extraction was implemented with a bi-directional laser chirp in order to simultaneously measure the velocity and range of moving targets. The utilization of both a laser up-sweep (blue line) and down-sweep (green line) disambiguates the range of a moving target that imparts a Doppler shift on backscattered light. The signed magnitude of the beat frequency difference is proportional to the velocity of the object, and the average to the range. The detections from the OPA LiDAR system are shown in Fig. 5(c), where a spinning umbrella is present in the scene. A spinning object is utilized as different object locations have varying velocity magnitudes and direction, depending on the distance to the center of rotation. This is clearly seen in Fig. 5(c) where half of the umbrella is moving towards the LiDAR system and half is moving away, both with increased magnitude away from the center of rotation. The data in the figure is before compensating the imparted Doppler shift so different "ranges" are detected for moving objects during the laser up-sweep and down-sweep. This is the first demonstration of velocity extraction from an OPA-based coherent ranging system and presents a major advantage of coherent LiDAR.

In Fig. 5, the range of the 2D LiDAR system was limited by the available indoor space and the system was taken outside during the daytime to test at longer ranges. Due to the coherent detection modality used, this LiDAR is inherently insensitive to ambient light, such as sunlight, so no performance degradation was expected, though no quantitative measurements of background light while testing can be provided at the moment.

Figure 6(a) shows an outdoor map of the test area and Fig. 6(b) is an image of the real-time data visualization used to display the returns processed by DSP on-board an FPGA. A frame rate of 10 Hz was used. Notable features are seen in the visualization such as parked cars, fence posts, and a pedestrian at 185 m. This demonstration is the first for coherent OPA LiDAR with the ability to achieve the long ranges (∼200 m) needed for many applications, such as autonomous vehicles, on real-world targets in an outdoor urban environment.

Finally, a coherent 3D LiDAR system was created with two active OPAs (with phase shifters). These OPAs are similar to those described in Section III. The components and real-time FPGA DSP in the previous 2D LiDAR system were used for detection. Each of the OPAs were independently calibrated and placed next to each other while set to repeatably raster scan a scene. Figure 7 shows an IR camera image of the scene and raster-scan pattern, and the 3D real-time visualization of the detections. Note that the rapid raster-scan causes frame-based aliasing in the output of the IR camera. A person at

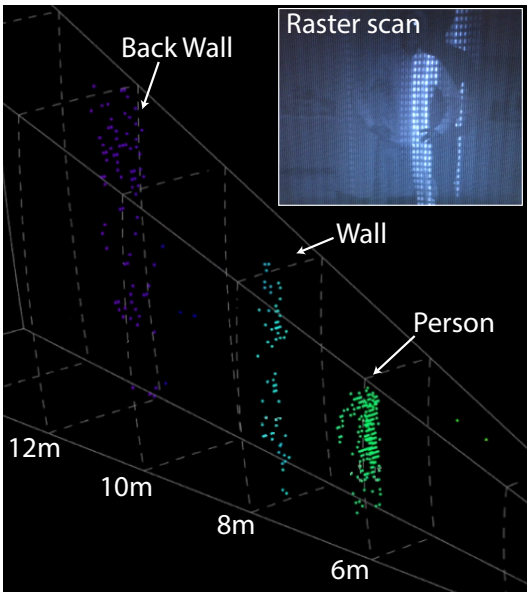

Fig. 7: Real-time data from a 3D LiDAR system consisting raster scanning OPAs (color is representative of range). Inset shows scene being raster scanned.

~7 m is clearly seen in the output 3D detections with notable features such as arms and legs with two separate walls behind them at ~8 m and ~12 m. This is the first realized real-time 3D LiDAR system with OPAs and shows the promise of this technology for solid-state LiDARs. Future iterations will focus on reducing the SWaP, for example reaching ~15 W power consumption to be vehicle compatible with increased integration. In addition, the longitudinal resolution is a function of the chirping bandwidth and can be increased by utilizing a different laser.

V. Optical Free-Space Data Communication

FSO communication has received significant interest for long-range direct line-of-sight applications in terrestrial and atmospheric settings [39]. However, current devices rely on discrete components which limits deployability in SWaP-C critical applications. The tight integration of silicon photonics with standard components such as traveling-wave Mach-Zehnder modulators (TW-MZM) [17], [40], [41], [42] makes steerable integrated OPAs a natural choice for the transmitter of an FSO link. There has been some work using OPAs for FSO communication but previously they have required lenses [21], [22], [23] for beam collimation. The receiver can be realized with commonly available top-illuminated avalanche photodetectors (APD) or a large aperture OPA. OPA receivers have the benefit of a larger "active area" than many APDs and the capability to couple the received light to an on-chip single-mode waveguide for further processing and detection by a small high-bandwidth photodetector. This enables data-rates that cannot be achieved with a large-area APD at the cost of a more directional receiver that must be actively steered towards the transmitter in dynamic-node systems. Furthermore, unlike an APD, an OPA receiver is insensitive to ambient light due to its directivity and relatively narrow-band operation.

In order to test the feasibility of OPA-based FSO links, initial links were demonstrated with a passive OPA transmitter. A block diagram of the experiment is shown in Fig. 8(a). An external laser was coupled to an external silicon photonics-based TW-MZM that was driven by a non-return-to-zero (NRZ) OOK pseudo-random bit sequence (PRBS) with an arbitrary waveform generator (AWG). The modulated optical signal was amplified with an erbium-doped fiber amplifier (EDFA) and coupled to a passive transmitter OPA. The main beam of the OPA transmitted across the room and back, using a mirror, for a total propagation length of 50 m to the receiver [Fig. 8(b)]. Two receivers were tested, a commercial-off-the-shelf APD and an identical OPA as the transmitter coupled to a fiber-based photodetector. Finally, the electrical output was analyzed with a sampling scope.

Figure 8(c) plots the received eye diagram when the APD was used as a receiver. A data-rate of 100 Mbps was achieved, limited by the cut-off frequency of the APD. Though this is a simple detection technique, utilizing an OPA as a receiver enables a higher bandwidth due to the capability to use

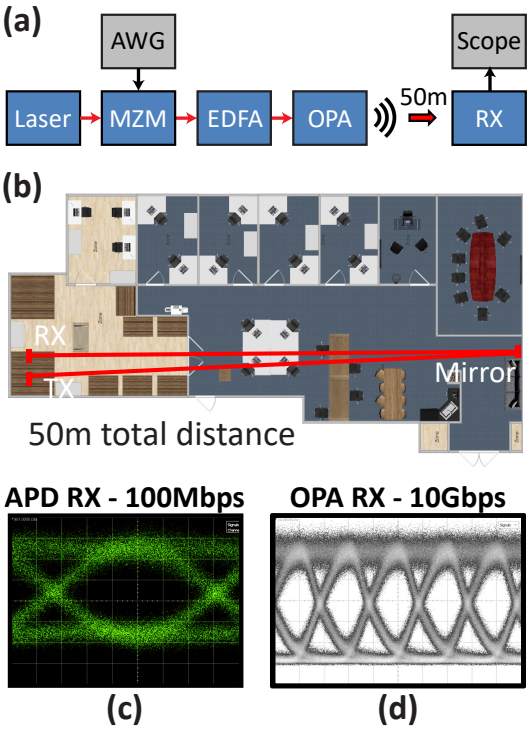

Fig. 8: (a) Experimental block diagram of a point-to-point 50 m link. (b) 50 m optical path from transmitting OPA to receiver. Received eye diagram (c) at 100 Mbps using an APD receiver and (d) at 10 Gbps using an OPA receiver.

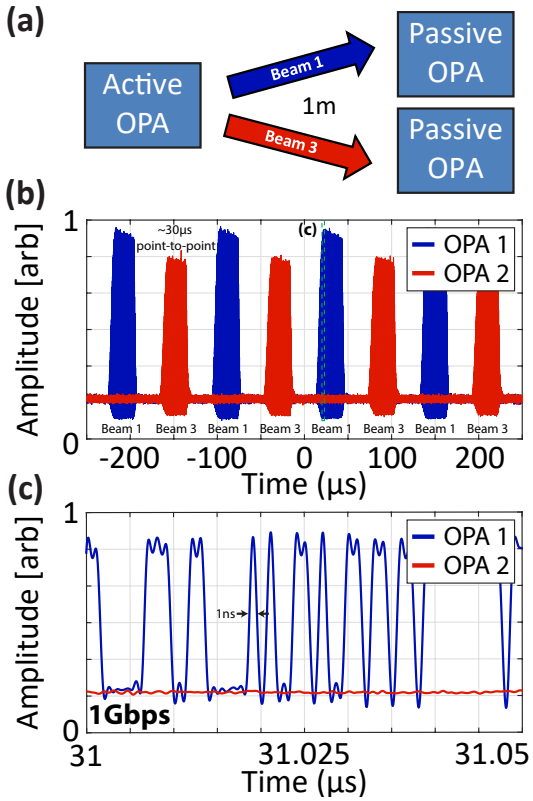

Fig. 9: (a) Experimental diagram of a point-to-multipoint 1 m link with an active TX OPA steering between two passive RX OPAs. (b) Received data sequences from RX OPA 1 and RX OPA 2. (c) Zoom in of the received data sequence.

compact single-mode photodetectors. A receiving OPA was manually aligned to accept the incoming transmitted beam. Figure 8(d) plots the resulting eye diagram with the RX OPA. A clean eye at 10 Gbps was observed for a record 50 m high-speed completely lens-free communication link with OPAs.

In the previous experiment, passive OPAs were used to demonstrate a static point-to-point communication link. Next, the transmitter was replaced with an active OPA similar to the one described in Section III to form a point-to-multipoint configuration. Two passive OPAs were used as receivers due to equipment constraints. However, they could easily be replaced with active OPAs to demonstrate a non-blocking communication network. Since they did not contain active phase control, both receivers were manually aligned to the transmit OPA at two different locations 1 m away. The transmit OPA was set to scan between four points, which in sequence were aligned to OPA 1, neither OPA, to OPA 2, and again neither OPA [Fig. 9(a)]. A settling time of $\sim$6 µs was achieved with a point-to-point sweep time of $\sim$30 µs. Similar to the previous experiment, laser light was modulated using an external modulator driven by an AWG producing a 1 Gbps NRZ OOK PRBS (bandwidth-limited by the real-time oscilloscope capturing the data) and amplified with an EDFA. The received light was amplified with an EDFA and input to a fiber-coupled photodetector. The result of this experiment is shown in Fig. 9(b) where packets of data from the TX OPA to the two RX OPAs are seen. Figure 9(c) zooms into a single block of data showing a clean 1 Gbps data transmission to the respective RX OPA. This demonstration is the first active lens-free OPA-to-OPA free-space optical link and shows the potential for high data-rate OPA-to-OPA-based communications in small-form-factor transceivers with integrated TW-MZMs and photodetectors.

VI. Conclusion

In conclusion, we have presented high-performance integrated optical phased arrays with applicable demonstrators in LiDAR and free-space data communication. Record performance and size has been attained through rigorous design and validated components in order to achieve low-power operation ($<$1 mW total), large field-of-views, and high-speed beam steering ($\sim$30 µs point-to-point). A steerable beam with a FWHM diffraction angle of 0.04° is demonstrated with 12 dB side lobe suppression and $<$25 dB noise floor for high power-in-main-beam efficiency. First-of-their-kind demonstrations were shown with real-time 2D and 3D coherent LiDAR systems with optical phased arrays. The 2D OPA LiDAR system measured diffuse targets at long-distance range of 185 m in an urban environment. The 3D OPA LiDAR system performed 2D raster scanning to range an indoor scene at $\sim$10m. Quantities such as max ranging distance, precision/resolution, and target reflectivity have not been fully characterized in these prototypes. Continued characterization is necessary to finalize these numbers. Furthermore, completely lens-free OPA-to-OPA free-space optical data-links were shown up to 50 m, including a point-to-multipoint link at 1 Gbps. This work presents the most advanced demonstrations of chip-scale beam steering to date, and shows the maturity of silicon photonic optical phased array technology, which has been enabled by advanced CMOS foundry processes. This technology has the capability to bring silicon photonics to new unique markets requiring optical beam steering with completely solid-state chip-scale devices fabricated on 300 mm silicon wafers.

Acknowledgments

The authors acknowledge all employees of Analog Photonics for their help and support in this work. The authors declare no competing interests.

References

[1] J. J. López, S. A. Skirlo, D. Kharas, J. Sloan, J. Herd, P. Juodawlkis, M. Soljačić, and C. Sorace-Agaskar, "Planar-lens enabled beam steering for chip-scale lidar," in *Conference on Lasers and Electro-Optics*. Optical Society of America, 2018, p. SM3I.1.

[2] Y. Wang, G. Zhou, X. Zhang, K. Yu, and M. C. Wu, "160x160 mems-based 2-d optical phased array," in *Conference on Lasers and Electro-Optics*. Optical Society of America, 2018, p. SM3I.3.

[3] D. N. Hutchison, J. Sun, J. K. Doylend, R. Kumar, J. Heck, W. Kim, C. T. Phare, A. Feshali, and H. Rong, "High-resolution aliasing-free optical beam steering," *Optica*, vol. 3, no. 8, pp. 887–890, Aug 2016.

[4] C. V. Poulton, M. J. Byrd, M. Raval, Z. Su, N. Li, E. Timurdogan, D. Coolbaugh, D. Vermeulen, and M. R. Watts, "Large-scale silicon nitride nanophotonic phased arrays at infrared and visible wavelengths," *Opt. Lett.*, vol. 42, no. 1, pp. 21–24, Jan 2017.

[5] K. V. Acoleyen, W. Bogaerts, J. Jágerská, N. L. Thomas, R. Houdré, and R. Baets, "Off-chip beam steering with a one-dimensional optical phased array on silicon-on-insulator," *Opt. Lett.*, vol. 34, no. 9, pp. 1477–1479, May 2009.

[6] K. V. Acoleyen, H. Rogier, and R. Baets, "Two-dimensional optical phased array antenna on silicon-on-insulator," *Opt. Express*, vol. 18, no. 13, pp. 13 655–13 660, Jun 2010.

[7] K. V. Acoleyen, W. Bogaerts, and R. Baets, "Two-dimensional dispersive off-chip beam scanner fabricated on silicon-on-insulator," *IEEE Photonics Technology Letters*, vol. 23, no. 17, pp. 1270–1272, Sept 2011.

[8] J. Sun, E. Timurdogan, A. Yaacobi, Z. Su, E. S. Hosseini, D. B. Cole, and M. R. Watts, "Large-scale silicon photonic circuits for optical phased arrays," *IEEE Journal of Selected Topics in Quantum Electronics*, vol. 20, no. 4, pp. 264–278, July 2014.

[9] J. Sun, E. Timurdogan, A. Yaacobi, E. S. Hosseini, and M. R. Watts, "Large-scale nanophotonic phased array," *Nature*, vol. 493, no. 7431, pp. 195–199, 2013.

[10] J. Sun, E. shah Hosseini, A. Yaacobi, D. B. Cole, G. Leake, D. Coolbaugh, and M. R. Watts, "Two-dimensional apodized silicon photonic phased arrays," *Opt. Lett.*, vol. 39, no. 2, pp. 367–370, Jan 2014.

[11] J. Sun, M. Moresco, G. Leake, D. Coolbaugh, and M. R. Watts, "Generating and identifying optical orbital angular momentum with silicon photonic circuits," *Opt. Lett.*, vol. 39, no. 20, pp. 5977–5980, Oct 2014.

[12] W. Guo, P. R. A. Binetti, C. Althouse, M. L. Maanovi, H. P. M. M. Ambrosius, L. A. Johansson, and L. A. Coldren, "Two-dimensional optical beam steering with inp-based photonic integrated circuits," *IEEE Journal of Selected Topics in Quantum Electronics*, vol. 19, no. 4, pp. 6 100 212–6 100 212, July 2013.

[13] J. C. Hulme, J. K. Doylend, M. J. R. Heck, J. D. Peters, M. L. Davenport, J. T. Bovington, L. A. Coldren, and J. E. Bowers, "Fully integrated hybrid silicon two dimensional beam scanner," *Opt. Express*, vol. 23, no. 5, pp. 5861–5874, Mar 2015.

[14] H. Abediasl and H. Hashemi, "Monolithic optical phased-array transceiver in a standard SOI CMOS process," *Opt. Express*, vol. 23, no. 5, pp. 6509–6519, 2015.

[15] S. Chung, H. Abediasl, and H. Hashemi, "A monolithically integrated large-scale optical phased array in silicon-on-insulator cmos," *IEEE Journal of Solid-State Circuits*, vol. 53, no. 1, pp. 275–296, Jan 2018.

[16] J. Notaros, N. Li, C. V. Poulton, Z. Su, M. J. Byrd, E. S. Magden, and M. R. Watts, "Cmos-compatible optical phased arrays with monolithically-integrated erbium lasers," in *Conference on Lasers and Electro-Optics*. Optical Society of America, 2018, p. STu4B.2.

[17] E. Timurdogan, Z. Su, C. V. Poulton, M. J. Byrd, S. Xin, R.-J. Shiue, B. R. Moss, E. S. Hosseini, and M. R. Watts, "Aim process design kit (aimpdkv2.0): Silicon photonics passive and active component libraries on a 300mm wafer," in *Optical Fiber Communication Conference*. Optical Society of America, 2018, p. M3F.1.

[18] C. V. Poulton, A. Yaacobi, D. B. Cole, M. J. Byrd, M. Raval, D. Vermeulen, and M. R. Watts, "Coherent solid-state lidar with silicon photonic optical phased arrays," *Opt. Lett.*, vol. 42, no. 20, pp. 4091–4094, Oct 2017.

[19] C. V. Poulton, D. Vermeulen, E. Hosseini, E. Timurdogan, Z. Su, B. Moss, and M. R. Watts, "Lens-free chip-to-chip free-space laser communication link with a silicon photonics optical phased array," in *Frontiers in Optics 2017*. Optical Society of America, 2017, p. FW5A.3.

[20] M. J. Byrd, C. V. Poulton, M. Khandaker, E. Timurdogan, D. Vermeulen, and M. R. Watts, "Free-space communication links with transmitting and receiving integrated optical phased arrays," in *Frontiers in Optics / Laser Science*. Optical Society of America, 2018, p. FTu4E.1.

[21] W. S. Rabinovich, P. G. Goetz, M. Pruessner, R. Mahon, M. S. Ferraro, D. Park, E. Fleet, and M. J. DePrenger, "Free space optical communication link using a silicon photonic optical phased array," pp. 93 540B–93 540B–6, 2015.

[22] T. Su, R. P. Scott, S. S. Djordjevic, N. K. Fontaine, D. J. Geisler, X. Cai, and S. J. B. Yoo, "Demonstration of free space coherent optical communication using integrated silicon photonic orbital angular momentum devices," *Opt. Express*, vol. 20, no. 9, pp. 9396–9402, Apr 2012.

[23] B. Guan, R. P. Scott, C. Qin, N. K. Fontaine, T. Su, C. Ferrari, M. Cappuzzo, F. Klemens, B. Keller, M. Earnshaw, and S. J. B. Yoo, "Free-space coherent optical communication with orbital angular, momentum multiplexing/demultiplexing using a hybrid 3d photonic integrated circuit," *Opt. Express*, vol. 22, no. 1, pp. 145–156, Jan 2014.

[24] F. Aflatouni, B. Abiri, A. Rekhi, and A. Hajimiri, "Nanophotonic coherent imager," *Opt. Express*, vol. 23, no. 4, pp. 5117–5125, Feb 2015.

[25] S. J. Spector, B. F. Lane, M. R. Watts, L. D. Benney, J. G. Delva, A. E. Hare, A. F. Kelsey, J. M. Mlynarczyk, E. S. Hosseini, C. V. Poulton, and J. P. Laine, "Broadband imaging and wireless communication with an optical phased array," in *Conference on Lasers and Electro-Optics*. Optical Society of America, 2018, p. SM3I.7.

[26] B. Abiri, R. Fatemi, and A. Hajimiri, "A 1-d heterodyne lens-free optical phased array camera with reference phase shifting," *IEEE Photonics Journal*, vol. 10, no. 5, pp. 1–12, Oct 2018.

[27] R. Fatemi, B. Abiri, and A. Hajimiri, "An 8x8 heterodyne lens-less opa camera," in *Conference on Lasers and Electro-Optics*. Optical Society of America, 2017, p. JW2A.9.

[28] F. Aflatouni, B. Abiri, A. Rekhi, and A. Hajimiri, "Nanophotonic projection system," *Opt. Express*, vol. 23, no. 16, pp. 21 012–21 022, Aug 2015.

[29] M. Raval, A. Yaacobi, and M. R. Watts, "Integrated visible light phased array system for autostereoscopic image projection," *Opt. Lett.*, vol. 43, no. 15, pp. 3678–3681, Aug 2018.

[30] C. V. Poulton, P. Russo, E. Timurdogan, M. Whitson, M. J. Byrd, E. Hosseini, B. Moss, Z. Su, D. Vermeulen, and M. R. Watts, "High-performance integrated optical phased arrays for chip-scale beam steering and lidar," in *Conference on Lasers and Electro-Optics*. Optical Society of America, 2018, p. ATu3R.2.

[31] A. Yaacobi, J. Sun, M. Moresco, G. Leake, D. Coolbaugh, and M. R. Watts, "Integrated phased array for wide-angle beam steering," *Opt. Lett.*, vol. 39, no. 15, pp. 4575–4578, Aug 2014.

[32] M. Zadka, Y.-C. Chang, A. Mohanty, C. T. Phare, S. P. Roberts, and M. Lipson, "On-chip platform for a phased array with minimal beam divergence and wide field-of-view," *Opt. Express*, vol. 26, no. 3, pp. 2528–2534, Feb 2018.

[33] K. Shang, C. Qin, Y. Zhang, G. Liu, X. Xiao, S. Feng, and S. B. Yoo, "Uniform emission, constant wavevector silicon grating surface emitter for beam steering with ultra-sharp instantaneous field-of-view," *Opt. Express*, vol. 25, no. 17, pp. 19 655–19 661, Aug 2017.

[34] M. Raval, C. V. Poulton, and M. R. Watts, "Unidirectional waveguide grating antennas with uniform emission for optical phased arrays," *Opt. Lett.*, vol. 42, no. 13, pp. 2563–2566, Jul 2017.

[35] C. T. Phare, M. C. Shin, J. Sharma, S. Ahasan, H. Krishnaswamy, and M. Lipson, "Silicon optical phased array with grating lobe-free beam formation over 180 degree field of view," in *Conference on Lasers and Electro-Optics*. Optical Society of America, 2018, p. SM3I.2.

[36] S. A. Miller, C. T. Phare, Y.-C. Chang, X. Ji, O. A. J. Gordillo, A. Mohanty, S. P. Roberts, M. C. Shin, B. Stern, M. Zadka, and M. Lipson, "512-element actively steered silicon phased array for low-power lidar," in *Conference on Lasers and Electro-Optics*. Optical Society of America, 2018, p. JTh5C.2.

[37] T. Komljenovic, R. Helkey, L. Coldren, and J. E. Bowers, "Sparse aperiodic arrays for optical beam forming and lidar," *Opt. Express*, vol. 25, no. 3, pp. 2511–2528, Feb 2017.

[38] D. Pierrottet, F. Amzajerdian, L. Petway, B. Barnes, G. Lockard, and M. Rubio, "Linear fmcw laser radar for precision range and vector velocity measurements," *MRS Proceedings*, vol. 1076, pp. 1076–K04, 2008.

[39] V. W. S. Chan, "Free-space optical communications," *J. Lightwave Technol.*, vol. 24, no. 12, pp. 4750–4762, Dec 2006.

[40] Z. Yong, S. Shopov, J. C. Mikkelsen, R. Mallard, J. C. Mak, S. P. Voinigescu, and J. K. S. Poon, "Flip-chip integrated silicon mach-zehnder modulator with a 28nm fully depleted silicon-on-insulator cmos driver," *Opt. Express*, vol. 25, no. 6, pp. 6112–6121, Mar 2017.

[41] M. Streshinsky, R. Ding, Y. Liu, A. Novack, Y. Yang, Y. Ma, X. Tu, E. K. S. Chee, A. E.-J. Lim, P. G.-Q. Lo, T. Baehr-Jones, and M. Hochberg, "Low power 50 gb/s silicon traveling wave mach-zehnder modulator near 1300 nm," *Opt. Express*, vol. 21, no. 25, pp. 30 350–30 357, Dec 2013.

[42] D. Patel, S. Ghosh, M. Chagnon, A. Samani, V. Veerasubramanian, M. Osman, and D. V. Plant, "Design, analysis, and transmission system performance of a 41 ghz silicon photonic modulator," *Opt. Express*, vol. 23, no. 11, pp. 14 263–14 287, Jun 2015.

Christopher V. Poulton Christopher V. Poulton is currently the Director of Photonic Integration at Analog Photonics. He received the B.S. degree in Electrical and Computer Engineering from the University of Colorado, Boulder, CO, in 2014 and the M.S. degree in Electrical Engineering from the Massachusetts Institute of Technology (MIT), Cambridge, MA, in 2016. He joined the Photonic Microsystems Group, MIT, as an NSF Fellow and an MIT Jacobs Irvine Fellow. There he was the Lead Researcher on the LIDAR effort of the DARPA E-PHI program, demonstrated the first coherent LIDAR with optical phased arrays and the first millimeter-scale optical phased array. He was awarded the Morris Joseph Levin Award for Outstanding Masterworks and was denoted a DARPA Riser. He has authored or co-authored more than 40 peer reviewed journal and conference publications along with several patents.

Matthew J. Byrd Matthew J. Byrd received the B.S. degree in Electrical Engineering from Clemson University, Clemson, SC, in 2015 and the M.S. in Electrical Engineering from the Massachusetts Institute of Technology, Cambridge, MA in 2017. He joined the Photonics Microsystems Group, MIT, leading the microwave photonics effort under the DARPA E-PHI program in 2016. Since graduation, he has worked at Analog Photonics as a member of the silicon photonics team developing integrated chip-scale LiDAR systems.

Peter Russo Peter Russo is Director of LiDAR at Analog Photonics. He received his Bachelor of Science in Electrical Engineering from University of Maryland, College Park in 2008. After graduating, he joined BAE Systems as part of the Engineering Leadership Development Program, through which he also received his Master of Science in Electrical Engineering from University of New Hampshire. At BAE Systems, he served as principle investigator on several active electro-optical systems programs. In 2015, he joined Formlabs, a 3D-printing startup, as a member of the electro-optical team.

Erman Timurdogan Erman Timurdogan is the Director of PDK development at Analog Photonics (AP). He is defining the roadmap and leading the documentation, design, and verification of APSUNY process design kit (PDK). His focus is electronic-photonic components for high-speed communications and low power systems. Before joining AP, he received his Ph.D. and M.S. in electrical engineering and computer science in 2016 from the Massachusetts Institute of Technology (MIT). During his studies at MIT, he demonstrated ultra-low power silicon modulators, a 3D integrated silicon electronic-photonic communication link, and the first silicon-based efficient second harmonic generator, all on 300mm silicon-on-insulator wafers. He authored over 65 peer-reviewed conference, journal publications and issued patents which were cited over 1000 times. He has 3 publications in Nature Publishing Group.

Murshed Khandaker Murshed Khandaker received his Bachelors degree in Electrical and Electronics Engineering from Bangladesh University of Engineering and Technology in September 1988 and his Masters in Electronics Engineering from Philips International Institute in June 1990. He has been working on digital signal processing firmware for LiDAR since joining Analog Photonics in May, 2017. Prior to joining Analog Photonics, he has worked on video processing and display drive electronics in Philips Electronics (1992–2004) and KOPIN Corporation (2005–2017) .

Diedrik Vermeulen Diedrik Vermeulen is currently the Director of Engineering at Analog Photonics. Diedrik has more than 10 years of experience in the field of commercializing silicon photonics technology. After his Ph.D. at Ghent University/IMEC where his work on Silicon Photonics Fiber-To-The-Home transceivers was commercialized by a university spin-off Caliopa, he joined Acacia Communications and worked there as a principal member of the silicon photonics team, bringing the first silicon photonics 100G CFP coherent transceiver to market for metro and long-haul applications. In 2015 he joined the Photonics Microsystems Group at MIT as a Research Scientist. Diedrik has authored and co-authored more than 50 papers and conference contributions in letters, journals and conferences and is the inventor of 15 patents.

Michael R. Watts Michael R. Watts is the President and Chief Executive Officer of Analog Photonics. He is also an Associate Professor of Electrical Engineer and Computer Science at MIT where he is the principal investigator of the DARPA E-PHI and DODOS programs. At MIT he demonstrated state-of-the-art silicon photonic devices such as electro-optic modulators, optical filters, and large-scale optical phased arrays on the first 300mm silicon photonics electronics-photonics with heterogenous integration of CMOS. Prior to MIT, he was a Principal Member of Technical Staff and Sandia National Labs where he led their silicon photonics effort. He is also the Chief Technology Officer of AIM Photonics, the $600M public-private partnership to advance the state of photonic manufacturing in the United States.